

**Microbiology:**

**An  $\alpha$ -Helical Core Encodes the Dual  
Functions of the Chlamydial Protein InCA**

Erik Ronzone, Jordan Wesolowski, Laura D.  
Bauler, Anshul Bhardwaj, Ted Hackstadt and  
Fabienne Paumet

*J. Biol. Chem.* 2014, 289:33469-33480.

doi: 10.1074/jbc.M114.592063 originally published online October 16, 2014

MICROBIOLOGY

MEMBRANE  
BIOLOGY

Access the most updated version of this article at doi: [10.1074/jbc.M114.592063](https://doi.org/10.1074/jbc.M114.592063)

Find articles, minireviews, Reflections and Classics on similar topics on the [JBC Affinity Sites](http://www.jbc.org/).

Alerts:

- [When this article is cited](#)
- [When a correction for this article is posted](#)

[Click here](#) to choose from all of JBC's e-mail alerts

This article cites 50 references, 22 of which can be accessed free at  
<http://www.jbc.org/content/289/48/33469.full.html#ref-list-1>

# An $\alpha$ -Helical Core Encodes the Dual Functions of the Chlamydial Protein Inca\*

Received for publication, June 25, 2014, and in revised form, September 24, 2014. Published, JBC Papers in Press, October 16, 2014, DOI 10.1074/jbc.M114.592063

Erik Ronzone<sup>†1,2</sup>, Jordan Wesolowski<sup>†1</sup>, Laura D. Bauler<sup>§</sup>, Anshul Bhardwaj<sup>¶</sup>, Ted Hackstadt<sup>§</sup>, and Fabienne Paumet<sup>‡3</sup>

From the Departments of <sup>‡</sup>Microbiology and Immunology and <sup>¶</sup>Biochemistry and Molecular Biology, Thomas Jefferson University, Philadelphia, Pennsylvania 19107 and the <sup>§</sup>Host-Parasite Interactions Section, Laboratory of Intracellular Parasites, Rocky Mountain Laboratories, NIAID, National Institutes of Health, Hamilton, Montana 59840

**Background:** The inclusion protein Inca inhibits and activates membrane fusion events during infection.

**Results:** *In vitro* assays and dominant negative *Chlamydia* mutants show that a protease-resistant core of Inca forms dimers and encodes both functions of Inca.

**Conclusion:** Inca forms stable coiled-coils to manipulate membrane fusion.

**Significance:** This project provides the most detailed understanding of how a chlamydial inclusion protein operates to manipulate membrane fusion.

*Chlamydia* is an intracellular bacterium that establishes residence within parasitophorous compartments (inclusions) inside host cells. Chlamydial inclusions are uncoupled from the endolysosomal pathway and undergo fusion with cellular organelles and with each other. To do so, *Chlamydia* expresses proteins on the surface of the inclusion using a Type III secretion system. These proteins, termed Incs, are located at the interface between host and pathogen and carry out the functions necessary for *Chlamydia* survival. Among these Incs, Inca plays a critical role in both protecting the inclusion from lysosomal fusion and inducing the homotypic fusion of inclusions. Within Inca are two regions homologous to eukaryotic SNARE (soluble N-ethylmaleimide-sensitive factor attachment receptor) domains referred to as SNARE-like domain 1 (SLD1) and SNARE-like domain 2 (SLD2). Using a multidisciplinary approach, we have discovered the functional core of Inca that retains the ability to both inhibit SNARE-mediated fusion and promote the homotypic fusion of *Chlamydia* inclusions. Circular dichroism and analytical ultracentrifugation experiments show that this core region is composed almost entirely of  $\alpha$ -helices and assembles into stable homodimers in solution. Altogether, we propose that both Inca functions are encoded in a structured core domain that encompasses SLD1 and part of SLD2.

*Chlamydia trachomatis* is the etiologic agent of human urogenital infection and of trachoma, the world's leading cause of infectious blindness (1). *Chlamydia* infection is the most frequently reported bacterial sexually transmitted disease in the United States, with ~1.4 million new cases reported annually

(Centers for Disease Control, United States). Failure to treat infections can result in tissue scarring, infertility, pelvic inflammatory disease, and ectopic pregnancy in females as well as permanent blindness in the case of ocular infections. Despite the availability of antibiotics to treat acute infections, *C. trachomatis* remains a significant medical and economic burden worldwide.

Members of the family *Chlamydiaceae*, including *C. trachomatis*, exhibit a characteristic two-stage developmental cycle as spore-like elementary bodies and as larger, metabolically active reticulate bodies. After internalization, elementary bodies differentiate into reticulate bodies, which proliferate inside a specialized membrane-bound compartment called an inclusion (2). The survival of *Chlamydia* depends on its ability to rapidly modify the nascent inclusion in order to (i) isolate it from the canonical endolysosomal pathway that normally leads to degradation and bacterial clearance, (ii) induce inclusion-inclusion (homotypic) fusion, and (iii) generate novel fusion events with host organelles to acquire nutrients (3–6). To accomplish these modifications, bacterial effectors known as inclusion membrane proteins (Incs)<sup>4</sup> are shuttled to and embedded in the inclusion membrane via a putative Type III secretion system (7, 8), where they play essential roles in pathogenicity, tissue tropism, and maintenance of inclusion integrity (9, 10).

Inca was one of the first Incs for which a role in pathogenesis was established (11–13). Inca is a ~30-kDa transmembrane protein that contains two putative  $\alpha$ -helical/SNARE-like domains, suggesting that this bacterial protein functionally mimics eukaryotic SNARE proteins (14, 15).

SNAREs are responsible for most membrane fusion events in eukaryotic cells. They are located on virtually every intracellular compartment and use specific  $\alpha$ -helical domains (SNARE motifs) to assemble into stable multimeric complexes and cat-

\* This work was supported, in whole or in part, by National Institutes of Health Grant R01-AI073486 (to F. P.).

<sup>†</sup> Both authors contributed equally to this work.

<sup>2</sup> Present address: Laboratories of Molecular Medicine, Brown University, Providence, RI 02903.

<sup>3</sup> To whom correspondence may be addressed: Dept. of Microbiology and Immunology, Thomas Jefferson University, 233 S. 10th St., BLSB Rm. 750, Philadelphia, PA 19107. Tel.: 215-503-8567; Fax: 215-923-4153; E-mail: fabienne.paumet@jefferson.edu.

<sup>4</sup> The abbreviations used are: Inc, inclusion membrane protein; CTD, C-terminal domain; NBD, nitrobenzoxadiazole; SLD, SNARE-like domain; pi, postinfection; Tet, anhydrotetracycline; TMD, transmembrane domain; VAMP, vesicle-associated membrane protein; Tricine, N-[2-hydroxy-1,1-bis(hydroxymethyl)ethyl]glycine (systematic); MOI, multiplicity of infection; pk1 and pk2, peak 1 and 2, respectively.

**TABLE 1**  
DNA primers used in this study  
All sequences are listed 5' to 3'.

Primer name	Sequence (5' → 3')	Reference/Source
FO160	GGGCATATCCATATGACAACGCCTACTCTAATCGTG	Ref. 22
FO440	CCGGAATTCATGGCAACGCCTACTCTAATC	Ref. 23
FO510	AAGGAAAAAGCGCCGCATGACAACGCCTACTCTAATC	This study
FO511	ACGCAGTCGACCTACTTGTTCATCGTCATCCTTGTAGTCGGAGCTTTTCTAGAGGG	This study
FO512	ACGCGTCGACCTACTTGTTCATCGTCATCCTTGTAGTCAGAATAAAAAATCTTGAGATAC	This study
FO515	CATGCCATGGCCACCGCTAATCTACATGTATAC	This study
FO516	CCGCTCGAGAAGAGTTTTAGAAAAGTTG	This study
FO527	CGCGGATCCTCAAAGAGTTTTAGAAAAGTTG	This study
FO538	ACGCGTCGACCTACTTGTTCATCGTCATCCTTGTAGTCAAGAGTTTTAGAAAAGTTGTGAAA	This study

alyze the fusion of the lipid bilayers on which they reside (16–18). In addition to their role in membrane fusion, certain SNARE proteins (known as inhibitory SNAREs, or i-SNAREs) are capable of suppressing certain fusion events to maintain organelle homeostasis (19). Thus, SNARE proteins constitute a universal membrane fusion machinery in eukaryotic cells and are prime targets for intracellular bacteria that need to establish residence inside host cells (20).

IncA has been shown to play a role in the homotypic fusion of inclusions (13). Microinjection of anti-IncA Fab fragments into *C. trachomatis*-infected cells and targeted mutation of the *incA* gene result in the accumulation of multiple, non-fused inclusions containing otherwise viable bacteria (13, 21). Recently, we have shown that IncA is also able to inhibit SNARE-mediated membrane fusion, likely to prevent fusion between the inclusion and the endocytic compartments (22, 23). Interestingly, clinical isolates of *C. trachomatis* lacking IncA display smaller inclusions and are significantly less virulent than IncA-positive strains (12, 24, 25).

In order to understand how IncA encodes both fusogenic and inhibitory functions, we previously studied the role of each SNARE-like domain contained in the protein (named SLD1 and SLD2; see diagram in Fig. 1A). We established that either SLD is capable of blocking host SNARE-mediated membrane fusion independent of the other; however, both domains are required to promote the homotypic fusion of inclusions (23).

In order to define the mechanism of action of IncA, we have now identified and characterized a trypsin-resistant region of IncA (the so-called IncA-Core) that spans the entire length of SLD1 and about one-third of SLD2. Limited proteolysis and circular dichroism experiments suggest that this region is highly structured and very stable. In addition, biochemical and cellular assays demonstrate that this region encodes the dual functions of the full-length wild type protein. The physiological relevance of these data were confirmed using *Chlamydia* expressing inducible wild type and dominant-negative IncA as FLAG-tagged proteins. Interestingly, IncA-Core predominantly forms dimers in solution, as compared with WT-IncA, which is mostly monomeric. However, during infection, both WT and IncA-Core form oligomers. This suggests that the C-terminal peptide that is missing in IncA-Core controls the oligomeric state of IncA and that a cellular and/or bacterial factor releases this peptide during infection for IncA to become fully fusogenic. The identification of the functional core of IncA provides the basis for a more comprehensive understanding of its mechanisms of action and could aid in the development of

novel therapeutics capable of interfering with its pathogenic function *in vivo*. Furthermore, such a structurally well defined region may be used to screen the proteomes of other intracellular bacteria, such as *Salmonella typhi* and *Mycobacterium tuberculosis*, for the presence of similar SNARE-like proteins.

## EXPERIMENTAL PROCEDURES

**Recombinant DNA and Cloning**—Tables 1 and 2 provide a summary of the primers and plasmids used in this study. The plasmid encoding the soluble C-terminal domain of IncA named ΔTMD-IncA (designated FD199) was described previously (23). The plasmid encoding IncA-Core was constructed by PCR-amplifying the region spanning Thr<sup>87</sup>–Leu<sup>237</sup> using primers FO515 and FO516 and FD201 (the plasmid encoding wild type full-length IncA) as template DNA. The PCR product was digested with NcoI and XhoI and ligated into pET28a (Thermo Scientific) digested with the same enzymes. The resulting plasmid was designated FD577. His<sub>6</sub>-tagged TMD-IncA-Core (residues 1–237) was PCR-amplified using primers FO160 and FO527 and FD201 as template DNA. PCR product was digested with NdeI and BamHI (Thermo Scientific) and ligated into pET28a. This construct was designated FD582. DsRed-TMD-IncA-Core was constructed by PCR-amplifying the region spanning Met<sup>1</sup>–Leu<sup>237</sup> using primers FO440 and FO527 and FD201 as template DNA. PCR products were digested with EcoRI and KpnI and ligated into pDsRed-monomer-C1 (kindly provided by Dr. Peter Antinozzi, Wake Forest School of Medicine). This construct was designated FD579. FD507 and FD509 (mammalian expression plasmids for IncA WT and SLD1, respectively) were described previously (23). pBOMB-IncA (also known as FD569) was constructed by amplifying the ORF of wild type IncA using primers FO510 and FO511. The PCR product was digested with NotI and SalI and ligated into the corresponding sites of pBOMB-tet-mCherry (26). pBOMB-SLD1 (also known as FD573) was constructed by amplifying residues 1–141 of wild type IncA using primers FO510 and FO512 and digesting and ligating as above. pBOMB-SLD2 (also known as FD576) was constructed by amplifying the ORF of IncA (mutant SLD1) using primers FO510 and FO511. FD472, described previously (23), was used as the DNA template. The mutations in this construct are I106D, F108A, F117A, F124A, T127D, V134D, F138A, and F145A. pBOMB-TMD-IncA-Core (FD588) was constructed by amplifying residues 1–237 of wild type IncA using primers FO510 and FO538 and digested and ligated into pBOMB-tet-

**TABLE 2**  
**Plasmids used in this study**

All plasmids carry the gene cassette encoding resistance to kanamycin unless stated otherwise.

Plasmid name	Relevant characteristics	Reference/Source
pET28a	IPTG-inducible expression of His <sub>6</sub> -tagged proteins in <i>E. coli</i>	Novagen
FD199	pET28 expression vector for Inca lacking N-terminal tail and transmembrane domain ( $\Delta$ TMD-Inca)	Ref. 23
FD201	pET28 expression vector for wild type Inca (Inca WT)	Ref. 22
FD577	pET28 expression vector for Inca-Core (residues 87–237)	This study
FD582	pET28 expression vector for TMD-Inca-Core (residues 1–237)	This study
DsRed-monomer-C1	Mammalian expression vector with N-terminal DsRed-monomer tag	Dr. P. Antinozzi (Wake Forest School of Medicine)
FD507	Mammalian expression vector for DsRed-tagged Inca WT (residues 1–273)	Ref. 23
FD509	Mammalian expression vector for DsRed-tagged SLD1 (residues 1–141)	Ref. 23
FD579	Mammalian expression vector for DsRed-tagged TMD-Inca-Core (residues 1–237)	This study
pBOMB-tet-mCherry	<i>C. trachomatis</i> vector expressing tetracycline inducible-mCherry; ampicillin-resistant	Ref. 26
FD569	pBOMB vector expressing wild type Inca-FLAG; ampicillin-resistant	This study
FD573	pBOMB vector expressing FLAG-Inca SLD1; ampicillin-resistant	This study
FD576	pBOMB vector expressing FLAG-Inca SLD2; ampicillin-resistant	This study
FD588	pBOMB vector expressing FLAG-TMD-Inca-Core; ampicillin-resistant	This study

mCherry as described above. Plasmids were sequenced at the Nucleic Acids Facility at Thomas Jefferson University.

**Protein Expression and Purification**—Expression plasmids for all recombinant constructs were transformed into BL21(DE3) *Escherichia coli* and grown in Luria-Bertani (LB) medium to an optical density (at 600 nm) of 0.5. Isopropyl  $\beta$ -D-1-thiogalactopyranoside was added to a final concentration of 0.2 mM and induced at 16 °C overnight. After centrifugation,  $\Delta$ TMD-Inca and Inca-Core bacteria pellets were then resuspended in Buffer A (200 mM NaCl, 50 mM phosphate, 10% (w/v) glycerol, pH 7.4) and purified as described (23). Proteins were resolved on a HiLoad 16/60 Superdex preparation grade 200 column (Amersham Biosciences) equilibrated with Buffer A containing 1 mM dithiothreitol (DTT). Protein-containing fractions were collected and concentrated.  $\Delta$ TMD-Inca was flash-frozen in liquid nitrogen and stored at –80 °C. Inca-Core peaks 1 and 2 were kept at 4 °C. The purity of each protein was assessed by SDS-PAGE and Coomassie Blue staining. Protein concentrations were determined by measuring the optical density at 280 nm.

**Limited Proteolysis and N-terminal Sequencing**—10  $\mu$ g of  $\Delta$ TMD-Inca in Buffer A supplemented with 1 mM DTT was incubated with varying mass ratios of trypsin in a total reaction volume of 15  $\mu$ l. Reactions were stopped by adding PMSF (Amresco) to a final concentration of 1 mM and protein sample buffer to a final SDS concentration of 2% (w/v) and boiling at 95 °C for 10 min. Reaction products were resolved by SDS-PAGE using 12% bisacrylamide glycine gels or commercial Tris-Tricine 10–20% acrylamide gels (Bio-Rad). Gels were revealed with Coomassie Blue staining.

For N-terminal sequencing, trypsin fragments were resolved by SDS-PAGE and transferred onto PVDF membranes using a standard transfer protocol (23). Regions of the PVDF membrane corresponding to the different fragments were excised and sent for sequencing at the Tufts University Core Facility (Boston, MA).

**Homology Modeling**—The amino acid sequence of *C. trachomatis* Inca spanning Ser<sup>76</sup>–Ser<sup>273</sup> was used as the query sequence in PHYRE2 (27). The Protein Data Bank file of the homology model was analyzed using Chimera (University of California, San Francisco).

**MARCOIL Analysis**—The entire amino acid sequence of *C. trachomatis* Inca was used as the query sequence in

MARCOIL (28). The sequence was scored against the 9FAM matrix with default settings.

**Circular Dichroism**—Proteins were diluted to 10  $\mu$ M in Buffer A supplemented with 1 mM DTT and analyzed in a 0.1-cm quartz cuvette (Starna) using a Jasco-810 spectropolarimeter. Wavelength scans were taken between 196 and 250 nm at 20 °C in the X-Ray Crystallography and Protein Characterization Core Facility at Thomas Jefferson University. For each replicate, five accumulations were taken and averaged. At least three replicate scans for each protein were performed. Raw data were normalized to the mean residue ellipticity ( $\Phi$ ) for each protein using the following equations,

$$\text{Mean residue weight (MRW)} = (\text{molecular weight}) / (\text{no. of residues} - 1) \quad (\text{Eq. 1})$$

$$\text{Mean residue ellipticity } (\Phi) = (\text{mdeg} \times \text{MRW}) / (\text{path length} \times \text{concentration}) \quad (\text{Eq. 2})$$

where the molecular mass is expressed in daltons, mdeg is the raw output data from the spectropolarimeter, the path length is expressed in mm, and protein concentration is expressed in mg/ml. The percentage secondary structure in each construct was calculated using the K2D3 algorithm (29).

**Analytical Ultracentrifugation**— $\Delta$ TMD-Inca, Inca-Core peak 1, and Inca-Core peak 2 obtained after size exclusion chromatography were diluted in Buffer A supplemented with 1 mM DTT to concentrations between 25 and 130  $\mu$ M and subjected to analytical ultracentrifugation analysis using a Beckman Coulter ProteomeLab XL-I analytical ultracentrifuge equipped with absorbance optics and an eight-hole An-50 Ti analytical rotor. Sedimentation equilibrium experiments were carried out at 4 °C by collecting absorption scans at a fixed wavelength of 278 nm and spinning samples at four different velocities of 12,000, 18,000, 24,000, and 30,000 revolutions/min. The program SEDNTERP version 1.09 was used to correct the experimental *s* value to standard conditions at 20 °C in water (*s*<sub>20,w</sub>) and to calculate the partial specific volume of each protein, solvent density, and relative viscosity values along with the theoretical molecular mass (30). Data were fit to a “species analysis” model available in the SEDPHAT program (31, 32).

## Functional Inca Core Region

Analysis was performed for each protein concentration separately, and the molecular masses were determined from the average obtained from the analyses of three protein concentrations.

**HeLa Transfection**—HeLa cells were cultured as described previously (23). Twenty-four hours prior to transfection, HeLa cells were seeded into either 6-well or 10-cm tissue culture plates in complete DMEM (DMEM supplemented with 2 mM L-glutamine, 10% fetal bovine serum (FBS), and 10  $\mu$ g/ml gentamicin) and grown to 80% confluence. Cells were transiently transfected in DMEM without antibiotics (DMEM supplemented with 2 mM L-glutamine and 10% FBS) with Lipofectamine 2000 according to the manufacturer's instructions using 0.5  $\mu$ g (6-well plate) and 3  $\mu$ g (10-cm dish) of DNA with a Lipofectamine/DNA ratio of 3.5:1. These conditions consistently led to an average of ~60% transfection. Six hours after the addition of Lipofectamine-DNA complexes, cells were reseeded into 24-well plates containing coverslips (1  $\times$  10<sup>5</sup> cells/well) or into 10-cm dishes (1.75  $\times$  10<sup>6</sup> cells/plate) in DMEM without antibiotics and incubated for an additional 18 h before infection. For immunofluorescence experiments, each construct was reseeded in duplicate.

**Transformation of Chlamydia**—*C. trachomatis* serovar L2 expressing FLAG-Inca (FD569), FLAG-SLD1 (FD573), FLAG-SLD2 (FD576), or FLAG-TMD-Inca-Core (FD588) under the control of the tetracycline promoter were generated as described (26).

**Immunoprecipitation**—HeLa cells were infected at an MOI of 10 with *Chlamydia* expressing different forms of FLAG-tagged Inca. 8 h postinfection, FLAG proteins were induced with 10 ng/ml anhydrotetracycline (Tet). The cells were lysed 24 h postinfection with lysis buffer (25 mM Tris, 150 mM NaCl, 1% Nonidet P-40, 1 mM EDTA, 10% glycerol, pH 7.4) containing protease inhibitors. Equal amounts of lysate were incubated with Protein G Plus-agarose beads prebound with anti-FLAG antibody (Pierce) overnight at 4 °C. The beads were thoroughly washed with lysis buffer by centrifugation and then boiled in SDS-containing buffer. The samples were then analyzed by Western blot using anti-Inca antibody as described (33).

**Analysis of Homotypic Fusion**—HeLa cells were seeded onto coverslips in 24-well plates and infected with *C. trachomatis* serovar L2 or transformed *Chlamydia* strains at an MOI of 10. The infection was synchronized by centrifugation at 900  $\times$  g for 15 min at 22 °C. To induce FLAG-tagged protein expression, Tet was added to a final concentration of 10 ng/ml 8 h postinfection. DMSO was used as a control. Twenty-four hours postinfection, the cells were fixed with 2% (v/v) paraformaldehyde in phosphate-buffered saline (PBS) at room temperature and stained with Hoechst for 30 min before being mounted onto glass slides. For cells infected with *Chlamydia* expressing FLAG-tagged proteins, the cells were permeabilized with permeabilization buffer (10% goat serum, 0.1% saponin, 0.1% BSA in PBS) for 30 min and then stained with anti-FLAG (Santa Cruz Biotechnology) and AlexaFluor647 (Invitrogen) antibodies prior to being mounted. The coverslips were then analyzed using a Nikon TiE inverted microscope with a 60 $\times$  oil immersion objective, and images were acquired using NIS Elements (Nikon). For each condition, fields were selected at random, and 100–200 infected cells were counted and scored for the

presence of multiple non-fused inclusions. For cells transfected with DsRed fusion proteins, only transfected and infected cells in the randomly chosen fields were scored.

**Liposome Fusion Assay**—Liposome fusion assays were performed as described (18, 22, 23). Briefly, t-SNARE acceptor liposomes were reconstituted with the late endocytic SNARE complex (His<sub>6</sub>-Stx7, His<sub>6</sub>-Stx8, and His<sub>6</sub>-Vti1b). v-SNARE donor liposomes (containing the FRET pair nitrobenzoxadiazole (NBD) and rhodamine) were reconstituted with His<sub>6</sub>-VAMP8 with or without His<sub>6</sub>-TMD-Inca-Core or His<sub>6</sub>-Inca WT. Following density gradient centrifugation, 45  $\mu$ l of acceptor liposome were incubated with 5  $\mu$ l of donor liposome at 37 °C for 2 h. NBD fluorescence was recorded every 2 min. Raw data were normalized to maximal fluorescence as described (34).

**Statistics**—Student's two-tailed *t* test was used to compare averages. Significant differences were designated as *p* values of <0.05; \*, *p* < 0.05; \*\*, *p* < 0.01; \*\*\*, *p* < 0.0001.

## RESULTS

**The C-terminal Domain (CTD) of Inca Is Enriched in  $\alpha$ -Helix/Coiled-coil Motifs**—Inca encodes two SNARE-like domains, SNARE-like domain 1 (SLD1) and SNARE-like domain 2 (SLD2) (23). Based on their homology with eukaryotic SNAREs, we expected that either SLD would be able to both block and induce fusion. However, we previously demonstrated that neither SLD is capable of carrying out the dual functions of Inca (23). This observation prompted us to search for the functional core responsible for *both* functions of Inca. The MARCOIL program was first used to determine the presence of coiled-coil motifs throughout the protein (28). Full-length Inca, including the N-terminal tail region (residues 1–34), the large hydrophobic TMD (residues 35–75), and the CTD (residues 76–273), was tested against the 9FAM matrix, which compares the sequence with a data set derived from nine families of coiled-coil-containing proteins. Consistent with previous observations, only the CTD contained coiled-coil motifs (Fig. 1A) (14, 15). No significant coiled-coil propensity was found in either the N-terminal tail or the TMD.

Next, we determined the  $\alpha$ -helical content within the CTD using circular dichroism. We purified His<sub>6</sub>-tagged recombinant Inca-CTD (referred to as  $\Delta$ TMD-Inca) spanning residues 76–273 (23).  $\Delta$ TMD-Inca was diluted to a final concentration of 10  $\mu$ M in Buffer A, and circular dichroism was measured (Fig. 1B).  $\Delta$ TMD-Inca showed local minima around 207 and 220 nm, demonstrating strong  $\alpha$ -helix formation. Quantification of secondary structure using the K2D3 algorithm showed that  $\Delta$ TMD-Inca is 60.55  $\pm$  0.22% helical.  $\beta$ -Sheet structure was negligible (<4%). Moreover, the ratio of the mean residue ellipticities at 220 and 207 nm ( $\Phi_{220\text{ nm}}/\Phi_{207\text{ nm}}$ ) was 1.090  $\pm$  0.002. Ratios of  $\geq$ 1.0 correlate with the presence of interacting  $\alpha$ -helices or coiled-coils, whereas non-interacting helices are associated with ratios <1.0 (35–40), suggesting that Inca has a propensity to oligomerize.

We then generated a structural model of  $\Delta$ TMD-Inca using the PHYRE2 server (27). This algorithm compares input sequences against a large data set of established protein struc-

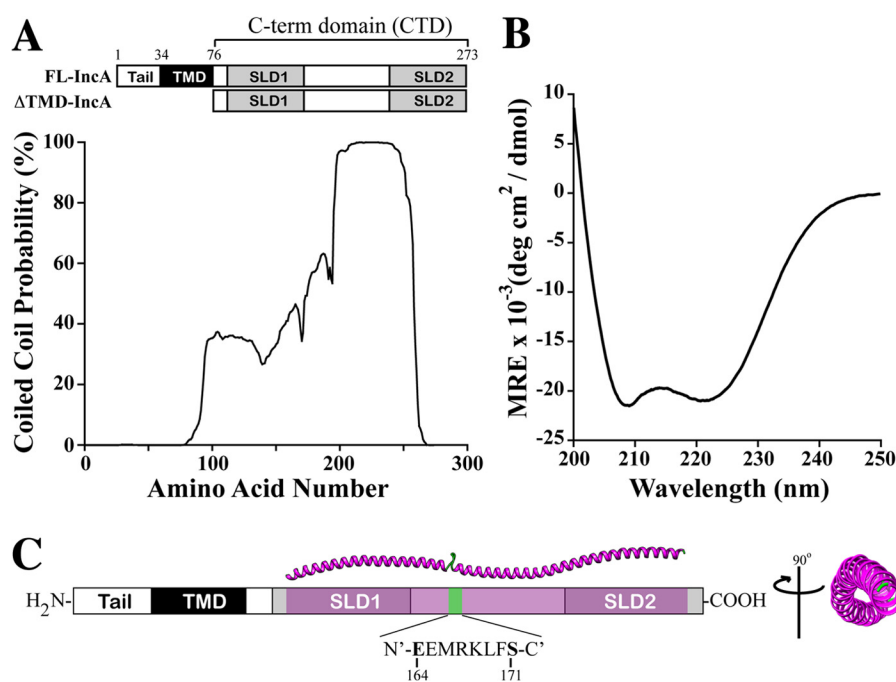


FIGURE 1. **Predicted coiled-coil regions within Inca.** *A*, the sequence of wild type Inca from *C. trachomatis* was analyzed using the MARCOIL program to identify putative coiled-coil domains. *Top*, schematic of wild type full-length Inca and  $\Delta$ TMD-Inca. The locations of residues on the MARCOIL plot approximate the locations shown on the diagram. *B*, circular dichroism analysis of  $\Delta$ TMD-Inca. Protein was diluted to 10  $\mu$ M in Buffer A with 1 mM DTT and analyzed on a Jasco 810 spectropolarimeter. The results shown are representative of three independent experiments. Double minima at 207 and 220 nm reveal high helical content. *C*, model of  $\Delta$ TMD-Inca monomer. Homology modeling was performed using the PHYRE2 server and the sequence corresponding to  $\Delta$ TMD-Inca. Purple areas represent  $\alpha$ -helices, and green ribbons represent unstructured regions. *Right*, model is rotated 90° to show the screw shape of  $\Delta$ TMD-Inca.

tures to arrive at a consensus three-dimensional structure for the protein sequence in question. The top hit for  $\Delta$ TMD-Inca was a model based on the structure of a C-terminal fragment of tropomyosin (Protein Data Bank entry 2EFR, 98.6% confidence, 11% identity), a dimeric coiled-coil protein involved in actin binding and muscle contraction (41). The model spanned almost the entire length of the C-terminal domain, encompassing most of SLD1 and SLD2 (Fig. 1C).  $\Delta$ TMD-Inca appears highly extended and contains a short unstructured region (represented by green ribbons) spanning Glu<sup>164</sup>–Ser<sup>171</sup> located in between the  $\alpha$ -helical domains SLD1 and SLD2 (purple ribbons). This model showed no  $\beta$ -sheet structure within the CTD as only  $\alpha$ -helices and random coils were present, which is consistent with the circular dichroism data (Fig. 1B). Collectively, these experiments demonstrate the strong presence of  $\alpha$ -helices and coiled-coils throughout the C-terminal domain of Inca.

**Limited Proteolysis of  $\Delta$ TMD-Inca Reveals a Stable Protected Core**—Previously, we observed a correlation between the loss of secondary structure in  $\Delta$ TMD-Inca and its loss of function, suggesting that tightly folded subdomain(s) exist within the CTD that probably encode Inca function (23). Thus, we mapped the folded regions of Inca by limited proteolysis because the folded domains encoding for Inca function should be protected from extensive proteolysis (42).  $\Delta$ TMD-Inca was incubated with increasing concentrations of trypsin for 30 min at 22 °C, and the resulting fragments were visualized by SDS-PAGE and Coomassie staining. As seen in Fig. 2A, in addition to the uncleaved  $\Delta$ TMD-Inca present at ~24 kDa, three discrete peptides ranging from ~6 to ~17 kDa were generated, among

which the ~17 kDa peptide appears the most prominent. Interestingly, after extended incubation of  $\Delta$ TMD-Inca overnight at 37 °C in the presence of trypsin, all bands were still visible, in particular the ~17 kDa band, indicating that these protected regions are highly stable.

Next, we determined the molecular weights of the three protected bands. To do so,  $\Delta$ TMD-Inca was treated with trypsin (1:30, w/w) or Buffer A for 30 min at 22 °C, and the products were resolved on a Tris-Tricine SDS acrylamide gradient gel. Migration distances for each band ( $R_f$ ) were calculated using ImageJ and normalized to the total migration distance (beginning of resolving gel to start of dye front,  $R_0$ ). The logarithm (base 10) of each molecular weight standard from the ladder was plotted as a function of its normalized migration distance ( $R_f/R_0$ ) (Fig. 2B, graph). The linear best fit curve ( $R^2 = 0.99468$ ) was used to determine the molecular weights of the digested fragments. The large fragment migrated with an  $R_f/R_0$  value of 0.86, corresponding to a molecular mass of 16.8 kDa. Similarly, we determined the molecular masses of the smaller fragments to be 8.04 and 7.11 kDa.

Edman degradation and sequencing were then used to identify the N-terminal cleavage sites of each peptide (43). Sequencing of the largest fragment revealed Lys<sup>86</sup> to be a target for trypsin cleavage (Fig. 2, B and C, Inca-Core). The 8.04 and 16.8 kDa fragments shared identical N termini, suggesting the low molecular weight fragments were degradation products of the 16.8 kDa fragment. In agreement with this hypothesis, sequencing of the 7.11 kDa band uncovered Arg<sup>167</sup> as a target for cleavage (Fig. 2, B and C). Interestingly, this residue is situated within

## Functional IncA Core Region

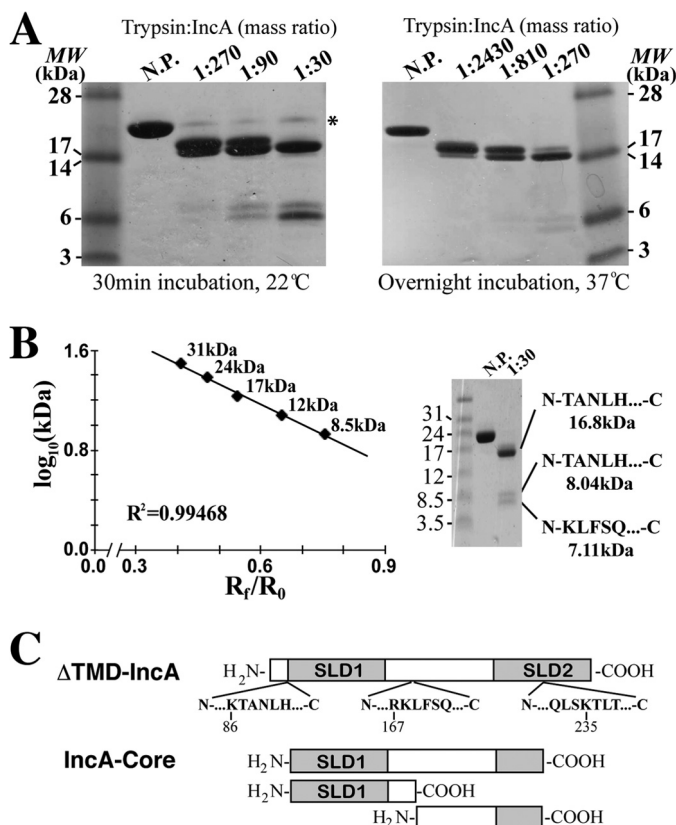


**FIGURE 2. Limited proteolysis of  $\Delta$ TMD-IncA.** A,  $\Delta$ TMD-IncA was incubated with increasing mass ratios of trypsin for 30 min at room temperature ( $\sim 22^\circ\text{C}$ ). Digestion products were resolved on SDS-PAGE and stained with Coomassie Blue. Three distinct bands appear after incubation with high concentrations of trypsin (1:270 trypsin/IncA mass ratio and above). \*, undigested protein. In parallel,  $\Delta$ TMD-IncA was incubated overnight in the presence of trypsin at the mass ratios listed. The presence of protected regions demonstrates the existence of a highly stable, structured core region within  $\Delta$ TMD-IncA. B, the molecular weights (MW) of the protected fragments were determined by their relative mobilities in SDS-PAGE by comparison against standards of known molecular weight (*Ladder lane*). The apparent molecular weights as well as the N-terminal sequencing results are shown *beside* the corresponding bands in the SDS-PAGE image (*right*). C, map of trypsin-susceptible residues in  $\Delta$ TMD-IncA. Sequencing results reveal Lys<sup>86</sup> and Arg<sup>167</sup> are targets of trypsin. Based on the molecular weight determination in B, Lys<sup>235</sup> is also a target for trypsin.

an unstructured region that was predicted by the homology model in Fig. 1C (*green ribbon*).

Analysis of the primary sequence revealed a trypsin cut site at position Lys<sup>235</sup> within SLD2 (Fig. 2C). Furthermore, the region spanning Thr<sup>87</sup>–Lys<sup>235</sup> has a theoretical molecular mass of 17.5 kDa, consistent with the calculated and apparent masses of the large fragment (Fig. 2, A and B). Thus, the large fragment generated by trypsin cleavage probably extends from Thr<sup>87</sup> well into SLD2 (Fig. 2C). Overall, limited trypsin digestion revealed a conformationally stable 16.8 kDa core consisting of a short, flexible linker region (N'–RKLFQS–C') flanked by SLD1 and one-third of SLD2.

*Ectopic Expression of IncA-Core Interferes with the Homotypic Fusion of Inclusions—In vivo*, IncA is involved in the homotypic fusion of inclusions (13). IncA likely mediates homotypic fusion via the formation of complexes that physically connect apposing inclusion membranes. In support of this hypothesis, it has been shown that ectopically expressed IncA,

which embeds in the endoplasmic reticulum in HeLa cells, inhibits the fusion of developing inclusions by forming cross-membrane interactions and titrating away endogenous IncA located on the inclusion (14). Thus, functional IncA that induces stable cross-membrane interactions (*e.g.* wild type IncA) will inhibit subsequent inclusion fusion when expressed ectopically by the host cell (14, 23, 44, 45). As such, if IncA-Core is functional during homotypic fusion, it should mediate cross-membrane interactions and recapitulate the function of wild type IncA. To assess IncA-Core functionality, HeLa cells were transfected with plasmids expressing either TMD-IncA-Core (IncA(1–237)), IncA WT (full-length IncA, positive control), or empty vector (negative control) prior to being infected at an MOI of 10 with *C. trachomatis* str. L2. Twenty-four hours postinfection, cells were analyzed for the presence of multiple non-fused inclusions using fluorescence microscopy. Compared with the empty vector (Fig. 3A, *top row*), the expression of TMD-IncA-Core (Fig. 3A, *bottom row*) results in the formation of multiple, non-fused inclusions. The frequency of these non-fused inclusions was significantly higher compared with the vector control (37% *versus* 12.8%) (Fig. 3A, *graph*). There is a difference in effect between IncA WT and TMD-IncA-Core, which could be due to different expression levels of the transfected IncA constructs. Alternatively, this difference may mean that residues between Leu<sup>237</sup> and Ser<sup>273</sup>, absent in TMD-IncA-Core but present in IncA WT, contribute to maximal IncA function or stability *in vivo*.

We expect that the ectopic expression of IncA and TMD-IncA-Core block homotypic fusion through the formation of oligomers between the ER and the inclusion membrane. Therefore, both of these proteins should be capable of forming highly structured dimers and/or oligomers. Using biophysical approaches, we then assessed the properties of both of these constructs. First, we cloned and expressed IncA-Core (residues Thr<sup>87</sup>–Leu<sup>237</sup>) as a C-terminal His<sub>6</sub>-tagged recombinant protein. Interestingly, size exclusion chromatography of  $\Delta$ TMD-IncA and IncA-Core revealed small yet consistent differences in the apparent hydrodynamic radii of the two proteins, with the smaller construct, IncA-Core (theoretical monomeric molecular mass, 17.4 kDa; Fig. 3B, *inset*), eluting as a major peak (pk1, 82 ml) followed by a minor peak (pk2, 94 ml) overlapping with the elution profile of  $\Delta$ TMD-IncA, which has a theoretical monomeric molecular mass of 23.7 kDa and elutes at 86 ml (Fig. 3B). We then analyzed the secondary and tertiary structures of IncA-Core.

We measured the circular dichroism (CD) of IncA-Core to determine the degree of helicity. Because this peptide is extremely protease-resistant, we expected that it would be highly structured. As shown in Fig. 3C, IncA-Core formed  $\alpha$ -helices in solution as determined by the presence of double minima around 207 and 220 nm. The lower overall mean residue ellipticity of IncA-Core compared with  $\Delta$ TMD-IncA suggested that the protein contained a higher proportion of helical residues than  $\Delta$ TMD-IncA (compare Figs. 3C and 1B). In fact, K2D3 analysis revealed that IncA-Core was  $86.71 \pm 0.47\%$  helical *versus*  $60.55 \pm 0.22\%$  for  $\Delta$ TMD-IncA. Not surprisingly, the percentage  $\beta$ -sheet structure in IncA-Core was very low ( $<1\%$ ). The increase in percentage helicity seen in IncA-Core is con-

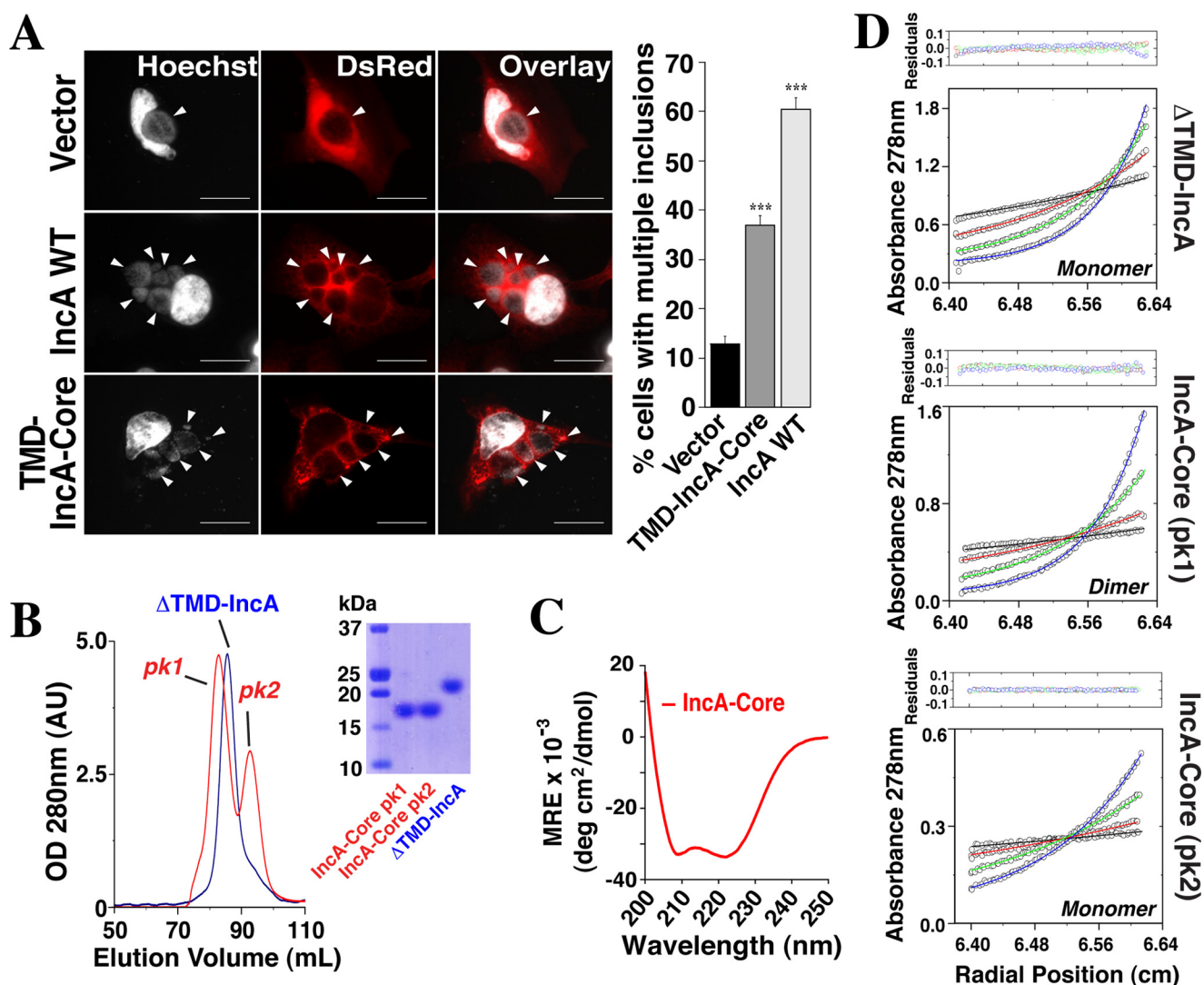


**FIGURE 3. Inca-Core forms dimers and blocks homotypic fusion.** *A*, ectopic expression of IncA-WT or IncA-Core inhibits subsequent inclusion development, leading to the presence of multiple, non-fused inclusions (white arrows). Vector control shows normal inclusion growth. Cells transfected with the indicated DsRed constructs (red) were infected with WT *Chlamydia* for 24 h prior to being fixed and stained with Hoechst to label nuclei and bacterial DNA (gray). These infected and transfected cells were then scored for the presence of multiple inclusions within the cell. The graph depicts the mean  $\pm$  S.D. (error bars) from four independent experiments conducted in duplicate; \*\*\*,  $p < 0.0001$ . For each replicate, an average of 130, 140, and 160 infected transfected cells were scored for DsRed (vector), DsRed-Inca, and DsRed-TMD-Core, respectively. *B*, size exclusion chromatography of proteins.  $\Delta$ TMD-Inca and IncA-Core ( $\sim 3$  mg/ml each) were analyzed by gel filtration in Buffer A supplemented with 1 mM DTT.  $\Delta$ TMD-Inca-Core (red curve) elutes as a major peak (pk1) at lower elution volume than  $\Delta$ TMD-Inca (blue curve), indicating a higher apparent hydrodynamic radius, which is followed by a minor peak (pk2). *Inset*, protein-containing fractions were pooled, concentrated, and run on SDS-PAGE to show that IncA-Core has a lower monomeric molecular weight than  $\Delta$ TMD-Inca. *C*, circular dichroism of IncA-Core. Purified IncA-Core was diluted to 10  $\mu$ M in Buffer A supplemented with 1 mM DTT. Wavelength scans are representative of three independent experiments. Double minima around 207 and 220 nm reveal high helical content. *D*, sedimentation equilibrium profiles of  $\Delta$ TMD-Inca (127  $\mu$ M), IncA-Core pk1 (85  $\mu$ M), and IncA-Core pk2 (50  $\mu$ M) were measured at four different rotor speeds of 12,000 (black), 18,000 (red), 24,000 (green), and 30,000 (blue) revolutions/min. Distributions were analyzed as part of a global fitting to the absorbance data at multiple rotor speeds for sample loading concentrations between 25 and 130  $\mu$ M (bottom panels). Solid lines are the global best fit to distributions denoted as circles, resulting in a molecular mass of  $23.9 \pm 0.8$ ,  $35.6 \pm 0.7$ , and  $18.2 \pm 0.8$  kDa for  $\Delta$ TMD-Inca (monomer), IncA-Core pk1 (dimer), and IncA-Core pk2 (monomer), respectively. The fidelity of fit is confirmed by the presence of very low residuals ( $<0.1\%$ ) (top panels).

sistent with the removal of unstructured regions from  $\Delta$ TMD-Inca.

We next investigated the oligomerization state of each construct. Analytical size exclusion chromatography is heavily biased by the shape of the protein. Therefore, we resorted to analytical ultracentrifugation as an alternative means of determining the oligomerization state of each protein.

Sedimentation equilibrium was used to analyze the oligomerization of  $\Delta$ TMD-Inca, IncA-Core pk1, and IncA-Core pk2 (Fig. 3D). Sedimentation equilibrium data at four different

rotor speeds were analyzed globally using the “species analysis” model in *SEDPHAT*. The resultant fit for  $\Delta$ TMD-Inca suggested a molecular mass of  $23.9 \pm 0.8$  kDa, consistent with a monomer (23.7 kDa). Interestingly, analysis of IncA-Core pk1 yielded a molecular mass of  $35.6 \pm 0.7$  kDa, consistent with a dimer (34.8 kDa), whereas IncA-Core pk2 resulted in a molecular mass of  $18.2 \pm 0.8$  kDa, consistent with a monomer (17.4 kDa). Even at relatively high concentrations (127, 130, and 100  $\mu$ M, respectively), the data fit to a “single-species” rather than a “two-species” model, thus ruling out any concentration-depen-

## Functional IncA Core Region

dent monomer/dimer equilibrium. This suggests that the monomeric form of IncA-Core could be a product of cotranslational protein misfolding, which does not undergo equilibrium with correctly folded IncA-Core dimer species. Nonetheless, given the predominant monomeric nature of  $\Delta$ TMD-IncA in solution, these data suggest that the dimerization of IncA may be regulated by the fragment of SLD2 that is present in  $\Delta$ TMD-IncA but missing in IncA-Core. Furthermore, through the formation of stable cross-membrane interactions, both IncA and IncA-Core are able to inhibit homotypic fusion when ectopically expressed in HeLa cells.

**IncA-Core Recapitulates the Dual Functions of IncA**—Due to the intractability of *Chlamydia* to genetic manipulation, the only approach to assess the function of IncA and its mutants during infection has been through ectopic expression in HeLa cells and indirect biochemical assays. However, recent advances in genetic tools now allow for the stable transformation of *Chlamydia* and the overexpression of secreted proteins, such as Incs (26). To determine whether IncA WT forms dimers/oligomers during infection and to assess the function of IncA-Core during infection, we generated *Chlamydia* clones that express FLAG-tagged TMD-IncA-Core under the control of the Tet promoter, which permits temporal regulation of effector protein expression. This strategy allows for different FLAG-IncA constructs to be overexpressed in parallel with endogenous IncA so as to not interfere with invasion or the early stages of infection due to aberrant IncA expression. These clones also constitutively express GFP, which enhances visualization. As controls, we generated FLAG-IncA WT, which is competent to mediate homotypic fusion, as well as FLAG-SLD1 and FLAG-SLD2 clones, which are unable to interfere with homotypic fusion when expressed ectopically in HeLa cells (23).

First, we infected HeLa cells with *Chlamydia* transformed with a plasmid encoding FLAG-IncA WT in the presence or absence of Tet. We then scored the cells for the presence of multiple, non-fused inclusions by immunofluorescence microscopy. As anticipated, FLAG-IncA WT is expressed on the surface of the inclusion in the presence of Tet (Fig. 4A, *IncA*, *DMSO* and *Tet*). Similar to the DMSO control, the overexpression of FLAG-IncA WT results in mostly single large fused inclusions (Fig. 4, A and B, *IncA* WT), whereas the overexpression of FLAG-SLD1 or FLAG-SLD2 blocks homotypic fusion (Fig. 4, A and B, *SLD1* and *SLD2*). Note that despite the expression of endogenous IncA (Fig. 4C, \*), we observed a significant increase in the percentage of cells with multiple non-fused inclusions when infected with FLAG-SLD1-expressing (50.3 versus 8.9%) and FLAG-SLD2-expressing (60 versus 14.5%) *Chlamydia*. This demonstrates that the overexpression of SLD1 and SLD2 acts in a dominant negative manner to alter inclusion morphology. Altogether, these data confirm that neither SLD is sufficient to mediate homotypic fusion.

Next, we infected HeLa cells with FLAG-TMD-IncA-Core *Chlamydia* in the presence or absence of Tet and assessed its impact on homotypic fusion. Similar to FLAG-IncA WT, ~80% of cells infected with FLAG-TMD-IncA-Core *Chlamydia* possess single large fused inclusions (Fig. 4, A and B, *TMD-IncA-Core*), although a slight increase in the number of cells with multiple inclusions in the presence of Tet (10 versus 19%) is

observed. This increase could be due to the enhanced dimerization and/or stability of IncA-Core (Fig. 3D). In total, these data show that IncA-Core retains its ability to mediate homotypic fusion and introduces a novel approach to dissecting Inc function during *Chlamydia* infection. Note that because both IncA WT and TMD-IncA-Core induce homotypic fusion to a similar extent, it is likely that the difference observed in the DsRed HeLa assay (Fig. 3A) is due to differences in expression level and or stability of the constructs.

Using these *Chlamydia* strains, we then assessed IncA oligomerization during infection by conducting a series of immunoprecipitation experiments. To do so, HeLa cells were infected with FLAG-TMD-IncA-Core, FLAG-SLD1, and FLAG-SLD2 expressing *Chlamydia*, and the binding of endogenous IncA to these FLAG-tagged proteins was assessed by immunoprecipitation and Western blot. As shown in Fig. 4D (left) endogenous IncA co-precipitated with FLAG-TMD-Core. Differences in molecular weight between endogenous IncA and these FLAG-IncA constructs enabled us to discriminate between these two proteins, which was not possible with endogenous IncA and FLAG-IncA WT. To assess IncA-IncA WT binding, we transfected HeLa cells with DsRed-IncA WT prior to infection with FLAG-IncA WT expressing *Chlamydia*. As controls, we also transfected cells with DsRed-TMD-IncA-Core (positive control) or DsRed (negative control). Twenty-four hours postinfection, FLAG-IncA WT was immunoprecipitated, and the binding of DsRed proteins was analyzed by Western blot using anti-IncA antibody. As shown in Fig. 4D (right), both DsRed-IncA WT and DsRed-TMD-Core co-precipitated with FLAG-IncA, demonstrating that although IncA WT is mostly a monomer in solution, it readily multimerizes during infection. Surprisingly, we also observed binding between SLD1 and IncA as well as between SLD2 and IncA, although neither of these two constructs is capable of inducing homotypic fusion. This suggests that similar to SNARE proteins, binding alone is not sufficient to generate membrane fusion (46–49).

In addition to mediating homotypic fusion, IncA has been shown to inhibit SNARE-mediated membrane fusion (22, 23). The inhibitory function of IncA is encoded entirely within the C-terminal domain and requires at least one intact SNARE-like domain (23). We validated the inhibitory capacity of IncA-Core using a well established liposome fusion assay (18). Recombinant human VAMP8 was reconstituted with or without IncA-WT or TMD-IncA-Core into donor liposomes containing the FRET pair NBD (nitrobenzoxadiazole) and rhodamine (Fig. 5, lanes 2–4 of inset). In parallel, recombinant human t-SNAREs syntaxin 7 (Stx7), syntaxin 8 (Stx8), and Vti1b were reconstituted into non-fluorescent acceptor liposomes (Fig. 5, lane 1 of inset). Following density gradient centrifugation, the two liposome populations were mixed at a 9:1 acceptor/donor volumetric ratio (total volume 50  $\mu$ l) and incubated at 37 °C for 2 h. Membrane fusion was measured as an increase in NBD fluorescence over time (34). Compared with the control (Fig. 5, black line), both IncA WT and TMD-IncA-Core significantly inhibited fusion, demonstrating that IncA-Core retains its ability to inhibit SNARE-mediated membrane fusion. Altogether, these results demonstrate that IncA-Core recapitulates the

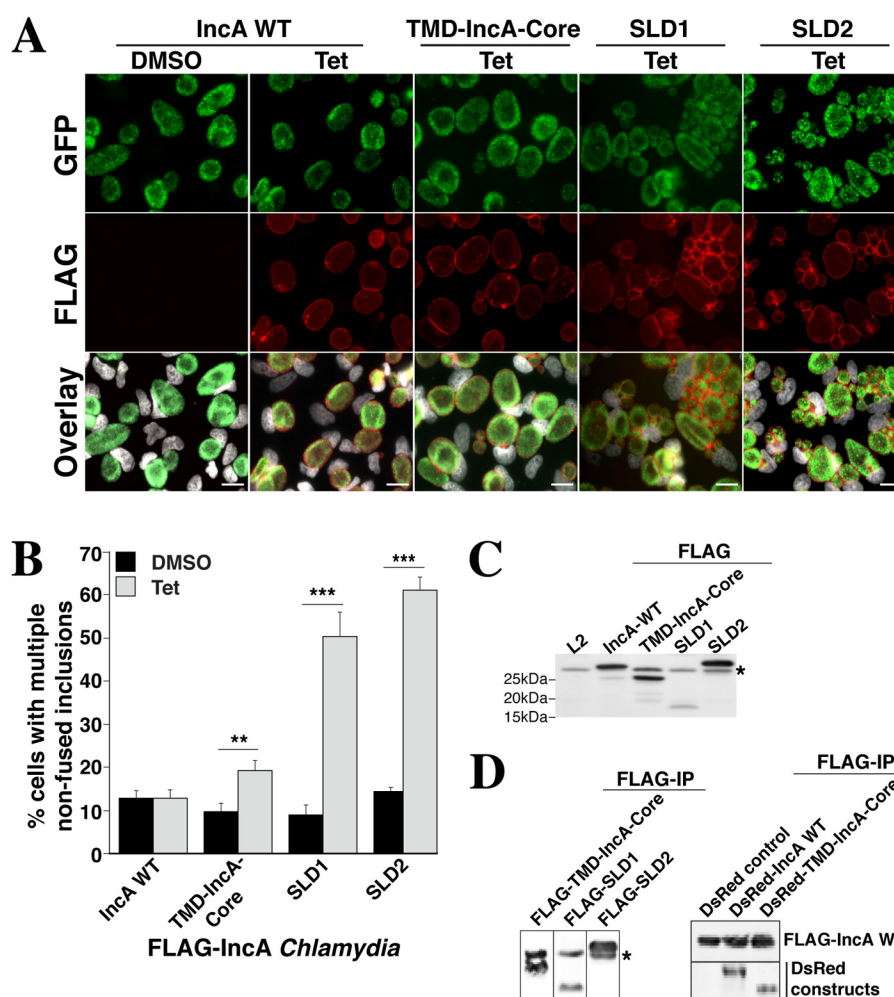


**FIGURE 4. IncA WT and TMD-IncA-Core mediate homotypic fusion in transformed *Chlamydia*.** A, HeLa cells were infected with *Chlamydia* overexpressing the indicated FLAG-tagged protein at an MOI of 10. FLAG fusion proteins were either not induced (DMSO) or induced with 10 ng/ml Tet at 8 h postinfection (pi). Twenty-four hours pi, cells were fixed and permeabilized. Cells were then stained with anti-FLAG/AlexaFluor647 antibodies (red), and nuclei were labeled with Hoechst (gray) prior to being analyzed by immunofluorescence microscopy. *Chlamydia* constitutively express GFP (green). FLAG-SLD1, IncA(1–141); FLAG-SLD2, full-length IncA with SLD1 inactivated by point mutations. Scale bar, 20  $\mu$ m. B, FLAG-SLD1 and FLAG-SLD2, but not FLAG-IncA WT or FLAG-TMD-IncA-Core, block homotypic fusion and generate multiple inclusions within the cell. Infected cells were scored for the presence of multiple inclusions within the cell. The graph depicts the mean  $\pm$  S.D. (error bars) from four independent experiments conducted in duplicate. \*\*,  $p < 0.01$ ; \*\*\*,  $p < 0.0001$ . For each experiment, an average of 250 infected cells were scored for FLAG-TMD-IncA-Core, FLAG-IncA WT, FLAG-SLD1, and FLAG-SLD2. C, endogenous IncA is still expressed following induction of FLAG-fusion proteins. Cells were infected with *Chlamydia* overexpressing the indicated FLAG protein at an MOI of 20. All samples were induced with 10 ng/ml Tet 8 h pi. Cells were lysed 24 h pi and analyzed by Western blot using anti-IncA antibody. L2, wild type *C. trachomatis* serovar L2. \*, endogenous IncA. The approximate molecular masses for WT IncA, TMD-IncA-Core, SLD1, and SLD2 are  $\sim$ 30,  $\sim$ 23,  $\sim$ 17, and  $\sim$ 32 kDa, respectively. D, left, TMD-IncA-Core binds endogenous IncA. HeLa cells were infected with FLAG-TMD-IncA-Core, FLAG-SLD1, or FLAG-SLD2 (MOI 10) followed by induction 8 h pi with 10 ng/ml Tet. Cells were lysed 24 h pi, and FLAG-tagged proteins were immunoprecipitated from equal amounts of cell lysate. Samples were analyzed by Western blot using anti-IncA antibody. \*, endogenous IncA. Right, IncA-IncA WT binding during infection. HeLa cells were transfected with empty DsRed vector control, DsRed-IncA WT, or DsRed-TMD-IncA-Core 24 h prior to being infected with FLAG-IncA WT-expressing *Chlamydia* (MOI 10). FLAG-IncA expression was induced 8 h pi with 10 ng/ml Tet. Cells were lysed 24 h pi, and FLAG-IncA was immunoprecipitated from equal amounts of cell lysate. Samples were analyzed by Western blot using anti-IncA antibody.

dual functions of IncA and identify, for the first time, the functional core of a SNARE-like bacterial protein.

## DISCUSSION

*C. trachomatis*-containing compartments avoid lysosomal fusion and undergo homotypic fusion to enhance infection. Mounting evidence suggests that the inclusion-bound protein IncA is at the intersection of these two processes, although it is unclear exactly how IncA accomplishes these tasks. Elucidating the structure of IncA will ultimately increase our understanding of how this protein performs its functions as well as aid in the identification of homologous effectors utilized by

other intracellular bacteria, such as *Salmonella* species and *M. tuberculosis*, which also manipulate host membrane fusion.

Here, we have identified a stable, protease-resistant core within IncA that encodes its dual functions. Our biophysical characterization of  $\Delta$ TMD-IncA and IncA-Core revealed that, although both constructs are clearly structured and enriched in  $\alpha$ -helices,  $\Delta$ TMD-IncA is mostly monomeric, whereas IncA-Core is mostly dimeric (Fig. 3). These data suggest that residues present in  $\Delta$ TMD-IncA that are absent in IncA-Core keep  $\Delta$ TMD-IncA in a monomeric conformation and that the loss of these residues results in IncA-Core dimerization (see model in Fig. 6).

## Functional IncA Core Region

$\Delta$ TMD-IncA encompasses SLD1 and SLD2 (residues 87–273), which are separated by a long linker region. Our limited proteolysis mapping experiment (Fig. 2) revealed that two-thirds of SLD2 (residues 236–273; Fig. 6A, *striped area*) are removed following exposure to trypsin. We hypothesize that residues within this region are involved in keeping  $\Delta$ TMD-IncA in its monomeric state (Fig. 6B, *left*) and that removal of this region permits the resulting protein (IncA-Core) to homodimerize (Fig. 6B, *right*).

Interestingly, intramolecular protein autoregulation has been demonstrated for SNARE proteins. In particular, the N-terminal region of the syntaxin family plays a role in the autoinhibition of SNARE complex formation, thus impacting the fusogenic state of the SNARE complex. For instance, Stx1A and Stx7 contain N termini that organize into three-helix bundles that fold back onto the SNARE domains of their respective syntaxin and inhibit ternary complex formation and membrane

fusion (50, 51). Upon stimulation, the N-terminal domain is released from the SNARE domain, and SNARE complex formation and membrane fusion proceed (50, 51). In the case of IncA, autoinhibition may act to keep IncA from prematurely forming dimers on the inclusion membrane. The removal or unfolding of the autoinhibitory region would then stimulate cross-membrane dimer formation, leading to the homotypic fusion of inclusions. The transition of IncA from a monomeric state into a dimeric state is likely regulated by host or bacterial proteins since the presence of  $\Delta$ TMD-IncA dimers in solution was minimal (Fig. 3), yet IncA-IncA binding was readily detectable during infection (Fig. 4D). Consistent with IncA dimerization/oligomerization in cells, chemical cross-linking of ectopically expressed IncA in HeLa cells followed by Western blotting revealed protein bands with apparent molecular weights consistent with IncA dimers and tetramers (14, 15). Our use of analytical ultracentrifugation allowed for the determination of the oligomeric state of IncA independent of chemical modifications and in isolation from other cellular proteins whose non-specific cross-linking to IncA could affect migration on SDS-PAGE. The fact that IncA-Core formed dimers in solution suggests that the tetramers seen by Western blot could be the result of over cross-linking of the dimeric form (14); however, we cannot exclude the possibility that high local concentrations of IncA on biological membranes lead to higher order oligomer formation or that regions of IncA outside of the CTD (e.g. in the N-terminal tail region) promote tetramerization *in vivo*.

The core region includes the majority of SLD1 and thus should inhibit fusion, as observed previously (22, 23). However, unlike  $\Delta$ TMD-IncA, which is predominantly monomeric, IncA-Core mostly forms a dimer in solution. Interestingly, the oligomeric state of IncA did not influence its inhibitory capacity, and TMD-IncA-Core is still able to block SNARE-mediated membrane fusion (Fig. 5). One possible mechanism is that binding to VAMP8 disrupts the IncA-IncA dimer, resulting in IncA-VAMP8 complex formation and blockage of the fusion event. Alternatively, IncA oligomers may directly bind to VAMP8, resulting in the formation of a stable four-helix bundle, structurally similar to SNARE complexes (17, 52). Additional studies will be necessary to discriminate between both of these possibilities.

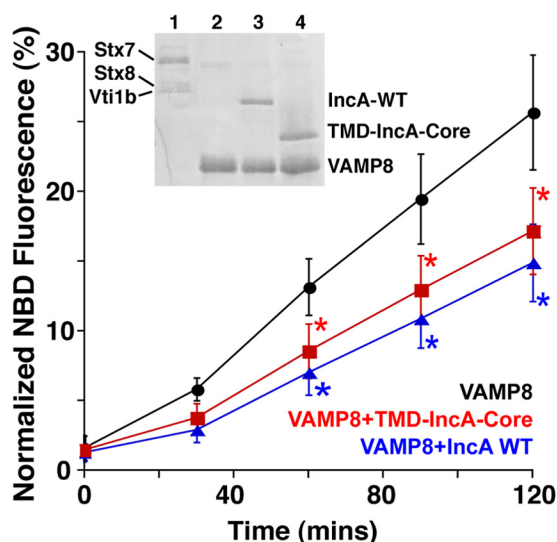


**FIGURE 5. TMD-IncA-Core inhibits late endocytic SNARE-mediated membrane fusion.** *Inset*, SDS-PAGE showing reconstitution of proteins into liposomes. VAMP8 was reconstituted into liposomes (*lane 2, inset*) with or without IncA WT (*lane 2, inset*) or TMD-IncA-Core (*lane 4, inset*) and mixed with liposomes reconstituted with the late endocytic t-SNARE complex (*lane 1, inset*). NBD fluorescence was measured every 2 min and plotted as normalized NBD fluorescence (see "Experimental Procedures"). Liposome fusion is inhibited by the presence of TMD-IncA-Core on VAMP8-containing liposomes. The graph depicts the mean  $\pm$  S.D. (error bars) from three independent experiments; \*,  $p < 0.05$ .

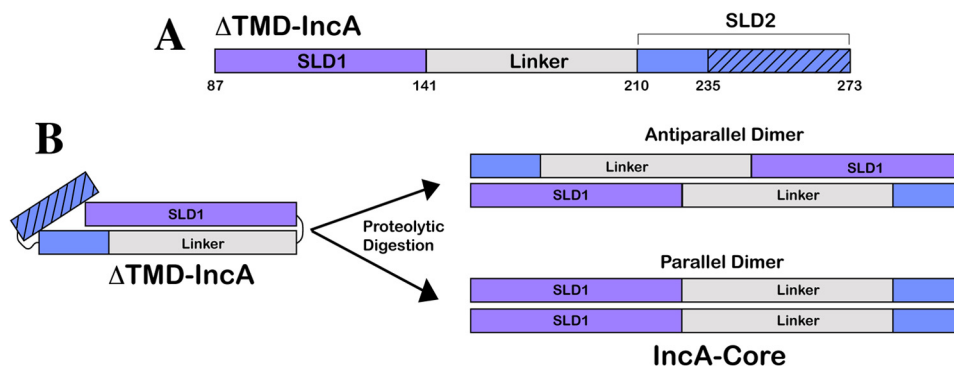


**FIGURE 6. Model of IncA dimerization.** *A*, diagram of  $\Delta$ TMD-IncA showing SLD1 and SLD2 separated by a linker region. *B*, a region of SLD2 (striped region, amino acids 235–273) keeps the protein in a monomeric conformation. Upon proteolytic digestion, this region is removed, and the resulting protein (IncA-Core; amino acids 87–235) undergoes a conformational change to a homodimer. In this model, the IncA-Core dimer could be an antiparallel (*top*) or parallel (*bottom*) homodimer.

Using both a well established HeLa assay and dominant negative Inca *Chlamydia* mutants, we showed that TMD-Inca-Core is fully competent to mediate the homotypic fusion of inclusions. The creation of *Chlamydia* strains expressing dominant-negative Inca constructs represents a novel and powerful tool to study the function of chlamydial effector protein. Using this new technology, we demonstrated that SLD1 or SLD2 alone was not sufficient to induce homotypic fusion, whereas Inca-Core, which displays an additional 94 amino acids compared with SLD1, is fully fusogenic. Homology modeling and circular dichroism analysis showed that Inca-Core consists almost exclusively of  $\alpha$ -helices, consistent with its homology to SNARE proteins. It is interesting to note that SLD1 and SLD2 are both able to bind Inca WT, although this binding does not translate into fusion. Altogether, these data suggest that either (i) a minimum size and a proper amino acid sequence is required to generate enough energy to induce membrane fusion, or (ii) the truncation and mutation of Inca resulted in the loss of one or several binding partner(s) necessary for Inca to enter into a fusion-competent complex.

In sum, the detailed structural analysis of Inca provides evidence that a highly structured core region of this bacterial effector (i) mediates cross-membrane interactions and homotypic fusion by forming stable coiled-coil multimers and (ii) retains its capacity to inhibit late endocytic SNARE-mediated membrane fusion. These data set the stage for future structural studies of Inca and other Inc proteins. If Inc SNARE-like proteins are key proteins for *Chlamydia* survival, it is possible that modulation or inhibition of Inc protein function by small molecules or drugs could represent a viable therapeutic option in the fight against infection. Indeed, our investigation into the ectopic expression of Inca mutants in infected HeLa cells as well as the generation of dominant negative Inca *Chlamydia* strains demonstrates the feasibility of engineering peptides that interact with endogenous Inca *in vivo*.

**Acknowledgments**—We thank Drs. Gino Cingolani, John Pascal, and Michael Root for critical discussion and advice during the course of this study. Research in this paper includes work carried out at the Sydney Kimmel Cancer Center X-ray Crystallography and Molecular Interaction Facility and Nucleic Acid Facility, which are supported in part by National Institutes of Health, NCI, Cancer Center Support Grant P30 CA56036.

## REFERENCES

- Weir, E., Haider, S., and Telio, D. (2004) Trachoma: leading cause of infectious blindness. *CMAJ* **170**, 1225
- Subtil, A., and Dautry-Varsat, A. (2004) Chlamydia: five years A. G. (after genome). *Curr. Opin. Microbiol.* **7**, 85–92
- Wyrick, P. B., and Brownridge, E. A. (1978) Growth of *Chlamydia psittaci* in macrophages. *Infect. Immun.* **19**, 1054–1060
- Wyrick, P. B., Brownridge, E. A., and Ivins, B. E. (1978) Interaction of *Chlamydia psittaci* with mouse peritoneal macrophages. *Infect. Immun.* **19**, 1061–1067
- Lawn, A. M., Blyth, W. A., and Taverne, J. (1973) Interactions of TRIC agents with macrophages and BHK-21 cells observed by electron microscopy. *J. Hyg.* **71**, 515–528
- Friis, R. R. (1972) Interaction of L cells and *Chlamydia psittaci*: entry of the parasite and host responses to its development. *J. Bacteriol.* **110**, 706–721
- Subtil, A., Parsot, C., and Dautry-Varsat, A. (2001) Secretion of predicted Inc proteins of *Chlamydia pneumoniae* by a heterologous type III machinery. *Mol. Microbiol.* **39**, 792–800
- Hsia, R. C., Pannekoek, Y., Ingerowski, E., and Bavoi, P. M. (1997) Type III secretion genes identify a putative virulence locus of *Chlamydia*. *Mol. Microbiol.* **25**, 351–359
- Rockey, D. D., Scidmore, M. A., Bannantine, J. P., and Brown, W. J. (2002) Proteins in the chlamydial inclusion membrane. *Microbes Infect.* **4**, 333–340
- Almeida, F., Borges, V., Ferreira, R., Borrego, M. J., Gomes, J. P., and Mota, L. J. (2012) Polymorphisms in inc proteins and differential expression of inc genes among *Chlamydia trachomatis* strains correlate with invasiveness and tropism of lymphogranuloma venereum isolates. *J. Bacteriol.* **194**, 6574–6585
- Rockey, D. D., Heinzen, R. A., and Hackstadt, T. (1995) Cloning and characterization of a *Chlamydia psittaci* gene coding for a protein localized in the inclusion membrane of infected cells. *Mol. Microbiol.* **15**, 617–626
- Suchland, R. J., Rockey, D. D., Bannantine, J. P., and Stamm, W. E. (2000) Isolates of *Chlamydia trachomatis* that occupy nonfusogenic inclusions lack Inca, a protein localized to the inclusion membrane. *Infect. Immun.* **68**, 360–367
- Hackstadt, T., Scidmore-Carlson, M. A., Shaw, E. I., and Fischer, E. R. (1999) The *Chlamydia trachomatis* Inca protein is required for homotypic vesicle fusion. *Cell Microbiol.* **1**, 119–130
- Delevoe, C., Nilges, M., Dautry-Varsat, A., and Subtil, A. (2004) Conservation of the biochemical properties of Inca from *Chlamydia trachomatis* and *C. caviae*: oligomerization of Inca mediates interaction between facing membranes. *J. Biol. Chem.* **279**, 46896–46906
- Delevoe, C., Nilges, M., Dehoux, P., Paumet, F., Perrinet, S., Dautry-Varsat, A., and Subtil, A. (2008) SNARE protein mimicry by an intracellular bacterium. *PLoS Pathog.* **4**, e1000022
- Söllner, T., Whiteheart, S. W., Brunner, M., Erdjument-Bromage, H., Geromanos, S., Tempst, P., and Rothman, J. E. (1993) SNAP receptors implicated in vesicle targeting and fusion. *Nature* **362**, 318–324
- Sutton, R. B., Fasshauer, D., Jahn, R., and Brunger, A. T. (1998) Crystal structure of a SNARE complex involved in synaptic exocytosis at 2.4 Å resolution. *Nature* **395**, 347–353
- Weber, T., Zemelman, B. V., McNew, J. A., Westermann, B., Gmachl, M., Parlati, F., Söllner, T. H., and Rothman, J. E. (1998) SNAREpins: minimal machinery for membrane fusion. *Cell* **92**, 759–772
- Varlamov, O., Volchuk, A., Rahimian, V., Doege, C. A., Paumet, F., Eng, W. S., Arango, N., Parlati, F., Ravazzola, M., Orci, L., Söllner, T. H., and Rothman, J. E. (2004) i-SNAREs: inhibitory SNAREs that fine-tune the specificity of membrane fusion. *J. Cell Biol.* **164**, 79–88
- Wesolowski, J., and Paumet, F. (2010) SNARE motif: A common motif used by pathogens to manipulate membrane fusion. *Virulence* **1**, 319–324
- Johnson, C. M., and Fisher, D. J. (2013) Site-specific, insertional inactivation of Inca in *Chlamydia trachomatis* using a group II intron. *PLoS One* **8**, e83989
- Paumet, F., Wesolowski, J., Garcia-Diaz, A., Delevoe, C., Aulner, N., Shuman, H., Subtil, A., and Rothman, J. (2009) Intracellular bacteria encode inhibitory SNARE-like proteins. *PLoS One* **4**, 1–9
- Ronzzone, E., and Paumet, F. (2013) Two coiled-coil domains of *Chlamydia trachomatis* Inca affect membrane fusion events during infection. *PLoS One* **8**, e69769
- Geisler, W. M., Suchland, R. J., Rockey, D. D., and Stamm, W. E. (2001) Epidemiology and clinical manifestations of unique *Chlamydia trachomatis* isolates that occupy nonfusogenic inclusions. *J. Infect. Dis.* **184**, 879–884
- Rockey, D. D., Viratyosin, W., Bannantine, J. P., Suchland, R. J., and Stamm, W. E. (2002) Diversity within inc genes of clinical *Chlamydia trachomatis* variant isolates that occupy non-fusogenic inclusions. *Microbiology* **148**, 2497–2505
- Bauler, L. D., and Hackstadt, T. (2014) Expression and targeting of secreted proteins from *Chlamydia trachomatis*. *J. Bacteriol.* **196**, 1325–1334
- Kelley, L. A., and Sternberg, M. J. (2009) Protein structure prediction on the Web: a case study using the Phyre server. *Nat. Protoc.* **4**, 363–371
- Delorenzi, M., and Speed, T. (2002) An HMM model for coiled-coil domains and a comparison with PSSM-based predictions. *Bioinformatics* **18**,

## Functional IncA Core Region

- 617–625
29. Louis-Jeune, C., Andrade-Navarro, M. A., and Perez-Iratxeta, C. (2011) Prediction of protein secondary structure from circular dichroism using theoretically derived spectra. *Proteins* 10.1002/prot.23188
  30. Hayes, D., Laue, T., and Philo, J. (1995) Sednterp: sedimentation interpretation program. University of New Hampshire, Durham, NH
  31. Schuck, P. (2005) in *Modern Analytical Ultracentrifugation: Techniques and Methods* (Scott, D. J., Harding, S. E., Rowe, A. J., eds) pp. 26–60, Royal Society of Chemistry, Cambridge
  32. Bhardwaj, A., Casjens, S. R., and Cingolani, G. (2014) Exploring the atomic structure and conformational flexibility of a 320 Å long engineered viral fiber using x-ray crystallography. *Acta Crystallogr. D Biol. Crystallogr.* **70**, 342–353
  33. Wesolowski, J., and Paumet, F. (2014) *Escherichia coli* exposure inhibits exocytic SNARE-mediated membrane fusion in mast cells. *Traffic* **15**, 516–530
  34. Parlati, F., Weber, T., McNew, J. A., Westermann, B., Söllner, T. H., and Rothman, J. E. (1999) Rapid and efficient fusion of phospholipid vesicles by the  $\alpha$ -helical core of a SNARE complex in the absence of an N-terminal regulatory domain. *Proc. Natl. Acad. Sci. U.S.A.* **96**, 12565–12570
  35. Cooper, T. M., and Woody, R. W. (1990) The effect of conformation on the CD of interacting helices: a theoretical study of tropomyosin. *Biopolymers* **30**, 657–676
  36. Graddis, T. J., Myszka, D. G., and Chaiken, I. M. (1993) Controlled formation of model homo- and heterodimer coiled coil polypeptides. *Biochemistry* **32**, 12664–12671
  37. Hodges, R. S., Semchuk, P. D., Taneja, A. K., Kay, C. M., Parker, J. M., and Mant, C. T. (1988) Protein design using model synthetic peptides. *Pept. Res.* **1**, 19–30
  38. Lau, S. Y., Taneja, A. K., and Hodges, R. S. (1984) Synthesis of a model protein of defined secondary and quaternary structure. Effect of chain length on the stabilization and formation of two-stranded  $\alpha$ -helical coiled-coils. *J. Biol. Chem.* **259**, 13253–13261
  39. Zhou, N. E., Kay, C. M., Sykes, B. D., and Hodges, R. S. (1993) A single-stranded amphipathic  $\alpha$ -helix in aqueous solution: design, structural characterization, and its application for determining  $\alpha$ -helical propensities of amino acids. *Biochemistry* **32**, 6190–6197
  40. Zhou, N. E., Zhu, B. Y., Kay, C. M., and Hodges, R. S. (1992) The two-stranded  $\alpha$ -helical coiled-coil is an ideal model for studying protein stability and subunit interactions. *Biopolymers* **32**, 419–426
  41. Jancsó, A., and Graceffa, P. (1991) Smooth muscle tropomyosin coiled-coil dimers. Subunit composition, assembly, and end-to-end interaction. *J. Biol. Chem.* **266**, 5891–5897
  42. Cleveland, D. W., Fischer, S. G., Kirschner, M. W., and Laemmli, U. K. (1977) Peptide mapping by limited proteolysis in sodium dodecyl sulfate and analysis by gel electrophoresis. *J. Biol. Chem.* **252**, 1102–1106
  43. Edman, P. (1949) Method for determination of the amino acid sequence in peptides. *Arch. Biochem.* **22**, 475
  44. Li, Z., Chen, C., Chen, D., Wu, Y., Zhong, Y., and Zhong, G. (2008) Characterization of fifty putative inclusion membrane proteins encoded in the *Chlamydia trachomatis* genome. *Infect. Immun.* **76**, 2746–2757
  45. Alzhanov, D., Barnes, J., Hruby, D. E., and Rockey, D. D. (2004) Chlamydial development is blocked in host cells transfected with *Chlamydia caviae* IncA. *BMC Microbiol.* **4**, 24
  46. Tsui, M. M., and Banfield, D. K. (2000) Yeast Golgi SNARE interactions are promiscuous. *J. Cell Sci.* **113**, 145–152
  47. Yang, B., Gonzalez, L., Jr., Prekeris, R., Steegmaier, M., Advani, R. J., and Scheller, R. H. (1999) SNARE interactions are not selective. *J. Biol. Chem.* **274**, 5649–5653
  48. Parlati, F., Varlamov, O., Paz, K., McNew, J. A., Hurtado, D., Söllner, T., and Rothman, J. E. (2002) Distinct SNARE complexes mediating membrane fusion in Golgi transport based on combinatorial specificity. *Proc. Natl. Acad. Sci. U.S.A.* **99**, 5424–5429
  49. McNew, J. A., Parlati, F., Fukuda, R., Johnston, R. J., Paz, K., Paumet, F., Söllner, T. H., and Rothman, J. E. (2000) Compartmental specificity of cellular membrane fusion encoded in SNARE proteins. *Nature* **407**, 153–159
  50. Dulubova, I., Sugita, S., Hill, S., Hosaka, M., Fernandez, I., Südhof, T. C., and Rizo, J. (1999) A conformational switch in syntaxin during exocytosis: role of munc18. *EMBO J.* **18**, 4372–4382
  51. Antonin, W., Dulubova, I., Arac, D., Pabst, S., Plitzner, J., Rizo, J., and Jahn, R. (2002) The N-terminal domains of Syntaxin 7 and Vti1b form three-helix bundles that differ in their ability to regulate SNARE complex assembly. *J. Biol. Chem.* **277**, 36449–36456
  52. Antonin, W., Fasshauer, D., Becker, S., Jahn, R., and Schneider, T. R. (2002) Crystal structure of the endosomal SNARE complex reveals common structural principles of all SNAREs. *Nat. Struct. Biol.* **9**, 107–111